Biochimica et Biophysica Acta 1828 (2013) 2134–2142

Contents lists available at SciVerse ScienceDirect

Biochimica et Biophysica Acta

journal homepage: www.elsevier.com/locate/bbamem

Effects of pyrenebutyrate on the translocation of arginine-rich cell-penetrating peptides through artificial membranes: Recruiting peptides to the membranes, dissipating liquid-ordered phases, and inducing curvature

Sayaka Katayama [a], Ikuhiko Nakase [a], Yoshiaki Yano [b], Tomo Murayama [a], Yasushi Nakata [c], Katsumi Matsuzaki [b], Shiroh Futaki [a,*]

[a] Institute for Chemical Research, Kyoto University, Uji, Kyoto 611-0011, Japan
[b] Graduate School of Pharmaceutical Sciences, Kyoto University, Sakyo-ku, Kyoto 606-8501, Japan
[c] HORIBA, Ltd, Minami-ku, Kyoto 601-8305, Japan

ARTICLE INFO

Article history:
Received 18 March 2013
Received in revised form 16 May 2013
Accepted 17 May 2013
Available online 24 May 2013

Keywords:
Arginine-rich cell-penetrating peptide
Oligoarginine
Pyrenebutyrate
Membrane fluidity
Lipid domain
Membrane curvature

ABSTRACT

Arginine-rich cell-penetrating peptides, including octaarginine (R8) and HIV-1 TAT peptides, have the ability to translocate through cell membranes and transport exogenous bioactive molecules into cells. Hydrophobic counteranions such as pyrenebutyrate (PyB) have been reported to markedly promote the membrane translocation of these peptides. In this study, using model membranes having liquid-ordered (Lo) and liquid-disordered (Ld) phases, we explored the effects of PyB on the promotion of R8 translocation. Confocal microscopic observations of giant unilamellar vesicles (GUVs) showed that PyB significantly accelerated the accumulation of R8 on membranes containing negatively charged lipids, leading to the internalization of R8 without collapse of the GUV structures. PyB displayed an alternative activity, increasing the fluidity of the negatively charged membranes, which diminished the distinct Lo/Ld phase separation on GUVs. This was supported by the decrease in fluorescence anisotropy of 1,6-diphenyl-1,3,5-hexatriene (DPH). Additionally, PyB induced membrane curvature, which has been suggested as a possible mechanism of membrane translocation for R8. Taken together, our results indicate that PyB may have multiple effects that promote R8 translocation through cell membranes.

1. Introduction

Recently, methodologies involving use of cell-penetrating peptides (CPPs) for intracellular delivery of membrane impermeable molecules have been developed [1–4]. These methodologies have gained considerable attention, especially for the intracellular delivery of bioactive macromolecules, including peptides, proteins, poly-nucleic acids and their derivatives. Among CPPs, those rich in arginine are among the most widely employed classes of CPPs, of which oligoarginines [1,4] and the HIV-1 Tat derived peptide (TAT peptide) [5,6] are representative examples. Chemical conjugation or fusion of CPPs with their payloads (or their stable non-covalent complex formation) results in efficient intracellular delivery.

The internalization mechanisms of arginine-rich CPPs include (i) direct translocation through plasma membranes and (ii) endocytosis followed by endosomal escape into cytoplasm. Arginine-rich CPPs may employ either or both mechanisms, depending on the administration conditions and physicochemical properties of the CPPs and payloads involved [7–9]. The former mechanism should be more efficient than the latter, and the contribution of the former process increases when the payload is of low molecular weight (typically, <5000–10,000).

To improve the efficacy of direct membrane translocation of arginine-rich CPPs and their payloads, we have developed an approach that uses hydrophobic counteranions including pyrenebutyrate (PyB) [10,11]. Treatment of cells with PyB in phosphate-buffered saline (PBS) followed by the addition of octaarginine (R8) or TAT typically leads to translocation of these CPPs into the cytosol within a few minutes, without observable membrane perturbation or cytotoxicity. Not only small molecular weight compounds, but also small proteins, including ubiquitin (8.6 kDa) [12] and green fluorescent protein (GFP) (28 kDa) [10], have been introduced into cells using this system. Although hydrophobic complex formation of arginine-rich CPPs with PyB and eventual internalization through

Abbreviations: BTLE, brain total lipid extract; Chol, cholesterol; CLSM, confocal laser scanning microscopy; CPP, cell-penetrating peptide; DMSO, dimethylsulfoxide; DOPC, dioleoylphosphatidylcholine; DOPS, dioleoylphosphatidylserine; DiD, 1,1′-dioctadecyl-3,3,3′,3′-tetramethylindodicarbocyanine; DPH, 1,6-diphenyl-1,3,5-hexatriene; Fmoc, 9-fluorenylmethyloxycarbonyl; GUV, giant unilamellar vesicle; LUV, large unilamellar vesicle; Ld, liquid disordered; Lo, liquid ordered; PyB, pyrenebutyrate; R8, octaarginine; SM, sphingomyelin; SRB, sulforhodamine B

* Corresponding author at: Institute for Chemical Research, Kyoto University, Uji, Kyoto 611-0011, Japan. Tel.: +81 774 38 3210; fax: +81 774 32 3038.
E-mail address: futaki@scl.kyoto-u.ac.jp (S. Futaki).

0005-2736/$ – see front matter © 2013 Elsevier B.V. All rights reserved.
http://dx.doi.org/10.1016/j.bbamem.2013.05.016

membranes, together with membrane potential, have been suggested as potential mechanisms [10,13], the details remain unclear.

Electrostatic interactions of arginine-rich CPPs with negatively charged molecules such as negatively charged lipids and proteoglycans have been considered a major factor driving the cell-surface adsorption of these peptides; this is supported by results from cell-based assays [14,15] and model systems [16–18]. Both we and others have reported that direct influx of oligoarginine peptides through the plasma membrane into cells does not occur uniformly across the cell surface. Rather, it occurs at specific sites on the membrane [9,19,20]. This has also been observed for PyB-mediated membrane translocation of R8 [10]. The preferential interaction of arginine-rich CPPs or other types of CPPs with membrane domains of high fluidity has been reported [21,22]; this might be explained by the nonuniformity of membrane lipid composition or the presence of micro-domains within the membrane. Therefore, we assessed the roles of PyB in promoting the internalization of arginine-rich CPPs by using simplified membrane models of giant unilamellar vesicles (GUVs) and large unilamellar vehicles (LUVs), featuring coexisting liquid-disordered (Ld) and -ordered (Lo) lipid phases. Understanding the roles of PyB in accelerated R8 uptake may lead to the development of more efficient and reliable delivery systems. The effects of pyrenebutyrate on peptide-membrane electrostatic interactions, lipid domain separation, membrane fluidity and curvature formation were thus analyzed.

2. Materials and methods

2.1. Reagents

1-Pyrenebutyric acid and 1,6-diphenyl-1,3,5-hexatriene (DPH) were purchased from Sigma-Aldrich Japan (Tokyo, Japan). Cholesterol (Chol) and organic solvents were from Wako Pure Chemical Industries (Osaka, Japan). 1,2-Dioleoyl-sn-glycero-3-phosphocholine (DOPC), 1,2-dioleoyl-sn-glycero-3-phospho-L-serine (DOPS), sphingomyelin (porcine brain, SM), brain total lipid extract (BTLE) (porcine), and Rhodamine-DOPE [18:1 Liss Rhod PE (=1,2-dioleoyl-sn-glycero-3-phosphoethanolamine-N-(Lissamine Rhodamine B sulfonyl) (ammonium salt)) were purchased from Avanti Polar Lipids (Alabaster, AL, USA). 1,1′-Dioctadecyl-3,3,3′,3′-tetramethylindodicarbocyanine (DiD) was purchased from Invitrogen (Life Technologies Japan, Tokyo, Japan). PyB was dissolved in dimethyl sulfoxide (DMSO) as a stock solution to give the concentration of 3 mM (for GUV experiments) and 20 mM (for LUV experiments), respectively.

2.2. Peptides

All the peptides used in this study have C-terminal amide structures and were chemically synthesized using Fmoc solid-phase peptide synthesis as previously reported [23]. For the preparation of fluorescently labeled peptides, a glycylcysteine sequence was placed to the C-terminus of the octaarginine segment and modified with Alexa Fluor 488 C_5 maleimide sodium salt or BODIPY FL N-(2-aminomethyl) maleimide (Life Technologies Japan, Tokyo, Japan) as already reported [23]. The actual sequences of the synthesized peptides are as follows: R8-Alexa, NH_2-$(Arg)_8$-Gly-Cys(Alexa488)-amide; hexanoyl-R8-Alexa, CH_3-$(CH_2)_4$-CO-$(Arg)_8$-Gly-Cys(Alexa488)-amide; R8W, NH_2-$(Arg)_8$-Trp-amide; R8, NH_2-$(Arg)_8$-amide; R8-BODIPY, NH_2-$(Arg)_8$-Gly-Cys(BODIPY)-amide. The structures of the synthesized peptides were confirmed by matrix-assisted laser desorption ionization time-of-flight mass spectrometry. Peptides were dissolved in PBS(−) (137 mM NaCl, 2.7 mM KCl, 8 mM Na_2HPO_4, 1.5 mM KH_2PO_4, pH 7.4) as stock solutions. Concentrations of fluorescent peptides were determined by absorbance measured using a Beckman DU 640 spectrophotometer with a molar extinction coefficient (ε) of 5690 cm^{-1} M^{-1} for tryptophan [24], 71,000 cm^{-1} M^{-1} for Alexa Fluor 488 [25], and 80,000 cm^{-1} M^{-1} for BODIPY FL [26], respectively.

2.3. Preparation of vesicles

2.3.1. GUVs

GUVs were prepared as described previously [20,27]. Briefly, type IX-A agarose (1% w/w) was coated on a glass-base dish (Iwaki, Tokyo, Japan) and dried on a hotplate (40 °C) for 1 h. Then, 1-mM chloroform solutions containing the respective lipids (5 μL) were spread on the agarose film and dried *in vacuo* for 20 min. PBS(−) containing 100 mM sucrose (200 μL) was gently added to the agarose-lipid film. The mixture was then left to stand for 3 h in the dark to allow hydration and swelling of the lipids. The supernatant was replaced with PBS(−) containing 100 mM glucose (150 μL) to yield GUVs with 100 mM sucrose and glucose in PBS(−) as the inner and outer solutions, respectively. When membranes were stained with DiD or Rhodamine-DOPE, lipid mixtures containing 0.5 mol% DiD or 2 mol% Rhodamine-DOPE were spread on agarose film. For the preparation of GUVs encapsulating sulforhodamine B (SRB), PBS(−) containing 100 mM sucrose and 20 μM SRB was employed for hydration of the lipids.

2.3.2. LUVs

LUVs were prepared as described previously [28]. Briefly, a chloroform solution containing the appropriate lipids was placed at the bottom of a flask and a lipid film was formed by rotary evaporation. After vacuum drying overnight, the lipid film was hydrated with PBS(−) and vortex-mixed to produce multilamellar vesicles (MLVs). The suspension was subjected to five freeze–thaw cycles and then extruded through polycarbonate filters (two filters, 100 nm pore size) using a LiposoFast extruder system (Avestin, Ottawa, Ontario, Canada) for 21 times. The concentration of LUVs was expressed as the lipid concentration, determined using a LabAssay Phospholipid kit (Wako).

2.4. CLSM observations of GUVs treated with peptides and PyB

Stock solutions of peptides (12 μM) in PBS(−) containing 100 mM glucose (25 μL) were added to the outer solution of GUVs PBS(−) containing 100 mM glucose (150 μL), as described in Section 2.3.1.; the time at which peptide solutions were added was defined as time zero. After 30 s, 0.12 mM PyB in PBS(−) containing 100 mM glucose and 4% DMSO (25 μL) was added to the appropriate final concentration. PBS(−) containing 4% DMSO (25 μL) was employed as a control for PyB. The peptide–GUV interaction was analyzed using a confocal laser scanning system (FV1000; Olympus) consisting of an inverted microscope (IX81; Olympus) equipped with a 20× UPlanSApo objective (dry, NA 0.75).

2.5. Fluorescence measurements

A RF-5300PC fluorescence spectrometer (Shimadzu, Kyoto, Japan) was employed, except for the anisotropy decay measurement. All measurements were obtained at 20 °C. The concentration of fluorescent molecules was set such that the inner filter effect was avoided.

2.5.1. Steady-state fluorescence anisotropy measurements of 1,6-diphenyl-1,3,5-hexatriene (DPH)

Fluorescence anisotropy measurements were acquired using a RF-5300PC fluorescence spectrometer equipped with polarizers. DPH in tetrahydrofuran (3 μL) was added to PBS(−) (1 mL) to a final concentration of 2 μM. R8 (4 μM) in 2 mM LUV solution (500 μL) and 20 mM PyB in DMSO (1 μL) dissolved in PBS(−) (500 μL) was successively added to the DPH solution. As a control, DMSO (1 μL) was used instead of 20 mM PyB. The mixtures were stirred gently for 30 min to equilibrate the distribution of DPH into lipid bilayers. Spectra were then recorded at excitation and emission wavelengths of 385 and 450 nm, respectively. Slit widths were 1.5 and 5 nm for excitation and emission, respectively.

The steady-state anisotropy (r) was calculated according to the equation:

$$r = \frac{I_{vv} - GI_{vh}}{I_{vv} + 2GI_{vh}}$$

where I represents the fluorescence intensity, and the two subscripts indicate the settings of the excitation and emission polarizers, respectively. v and h refer to the vertical and horizontal orientations, respectively. G is an instrumental correction factor, which is the ratio of the sensitivities of the individual detection systems. The G-factor can be determined according to the equation:

$$G = \frac{I_{hv}}{I_{hh}}.$$

G-factors were measured for each sample and anisotropy values were corrected.

2.5.2. Time-resolved fluorescence anisotropy measurement (fluorescence anisotropy decay) of R-BODIPY

Fluorescence anisotropy decay was measured using a time-correlated single-photon counting method on a HORIBA FluoroCube 3000U fluorescence lifetime spectrofluorometer equipped with polarizers and a light source with the appropriate wavelength for excitation. The pulse rate of excitation was 1 MHz. Data were analyzed using the DAS6 Fluorescence Decay Analysis Software (HORIBA). PyB (20 mM) in DMSO (0.5 μL) was dissolved in PBS(−) (500 μL) and mixed with 2 μM R8-BODIPY in LUVs (lipid concentration 1 mM) (500 μL) to yield final concentrations of 1 μM peptide, 10 μM PyB and 500 μM LUVs. As a control, DMSO (0.5 μL) was used instead of 20 mM PyB. Samples were mixed gently by pipetting. Detailed instrument settings are listed in Table 1.

The time-resolved anisotropy decay $r(t)$ is expressed by the equation [29]:

$$r(t) = \frac{I_{vv}(t) - GI_{vh}(t)}{I_{vv}(t) + 2GI_{vh}(t)}$$

where $I_{vv}(t)$ and $I_{vh}(t)$ represent the parallel and perpendicular polarized components of the fluorescence, respectively, after excitation by vertically polarized light. G represents the instrument-dependent factor for the anisotropy sensitivity, which is expressed as follows:

$$G = \int_0^\infty I_{hv}(t)dt / \int_0^\infty I_{hh}(t)dt$$

where $I_{hv}(t)$ and $I_{hh}(t)$ are the fluorescence intensities of the vertical and horizontal components after excitation by horizontally polarized light.

Generally, $r(t)$ can be described as multi-exponential decay:

$$r(t) = r_\infty + \sum_j r_{0j} \exp\left(-t/\theta_j\right)$$

where r_∞ is limiting anisotropy, θ_j represents individual correlation time, and r_{0j} represents the fractional anisotropy that decays with correlation time θ_j. The fluorescence anisotropy decay $r(t)$ was determined by least-square fitting of single or double exponential decay.

3. Results and discussion

3.1. Preferential adsorption of octaarginine (R8) on GUVs containing negatively charged lipids

Previous reports using artificial membranes have demonstrated the preferential accumulation of arginine-rich CPPs including TAT on negatively charged membranes [30–33]. Prior to investigating the mechanism by which PyB accelerates translocation of arginine peptides through plasma membranes using simplified artificial membranes, we first confirmed the preferential accumulation of arginine peptides on negatively charged membranes. Considering the heterogeneity of plasma membranes and the possible effects on membrane adsorption and translocation of arginine peptides, we employed simplified membrane models featuring coexisting liquid-disordered (Ld) and -ordered (Lo) lipid phases. DOPC and DOPS were employed as neutral and negatively charged lipids, respectively. GUVs composed of DOPC/SM/Chol (2:2:1) and DOPC/DOPS/SM/Chol (1:1:2:1) were prepared as examples of neutral and negatively charged artificial membranes, respectively [16,30,34,35]. Alexa Fluor 488-labeled octaarginine peptide (R8-Alexa) was employed as a representative arginine-rich CPP, and the modes of peptide interaction with membranes were visualized by CLSM (Fig. 1). Phase separation was

Table 1
Anisotropy decay of R8-BOPIPY.

Condition[a]		Exponential[b]	θ (ns)		S.D.	Fractional amplitude	Relative amplitude[c]	Average θ	χ^2
	PyB								
PBS	−	1		0.777	0.030	–	–	0.777	0.93
	+	1		0.931	0.031	–	–	0.931	1.13
		2	θ_1	4.776	0.550	0.00012	1.07	0.695	1.02
			θ_2	0.689	0.0710	0.0076	98.93		
DOPC 100%	−	1		0.584	0.0450	–	–	0.584	0.99
	+	1		0.800	0.0830	–	–	0.800	0.98
		2	θ_1	3.318	0.0770	0.010	43.52	0.981	0.98
			θ_2	0.634	0.0110	0.070	56.48		
DOPC/DOPS (80/20)	−	2	θ_1	4.718	0.588	0.087	88.01	2.039	1.15
			θ_2	0.416	0.0420	0.14	11.99		
	+	2	θ_1	7.904	1.428	0.084	94.99	4.018	1.14
			θ_2	0.390	0.048	0.073	5.01		

[a] R8-BODIPY, 1 μM; PyB, 10 μM, Lipid, 500 μM.

[b] In PBS(−) or in the presence of neutral DOPC LUVs, data were well fitted by one exponential approximation. In the presence of DOPC/DOPS (4:1) LUVs, data were not fitted by one exponential analysis and thus two-exponential fittings were employed. For comparison, the θ values analyzed by two exponential fittings in PBS(−) and DPPC LUVs were also provided.

[c] Relative amplitude was calculated as follows;

T1(channel) * B1 + T2(channel) * B2 = S

where T1 and T2 are each channel of component, and B1 and B2 are each fractional amplitude. Relative amplitude of T1 = T1 * B1 / S * 100.

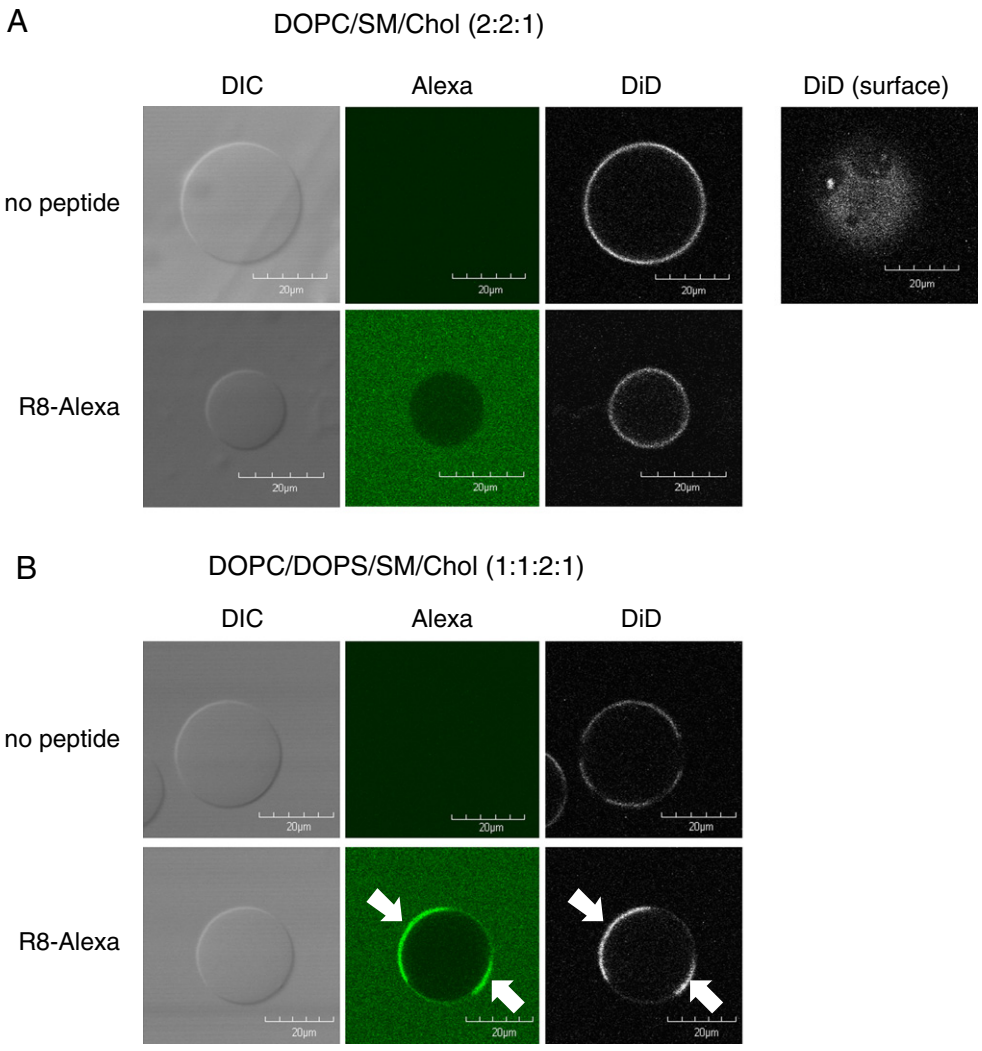

Fig. 1. Preferential accumulation of R8-Alexa on the liquid-disordered (Ld) phase of negatively charged GUVs. GUVs, composed of DOPC/SM/Chol (2:2:1) (A) or DOPC/DOPS/SM/Chol (1:1:2:1) (B), were incubated with peptides (1.5 μM) for 1 h and analyzed by CLSM. GUVs contain 0.5 mol% DiD as a Ld-phase marker. Although distinct separation of the liquid-ordered (Lo) and Ld phases was not observed in the cross-section of DOPC/SM/Chol GUV, the image focused on the GUV surface (right) shows the phase separation. Arrows in B indicate the colocalization of Alexa488 and DiD signals. Scale bar, 20 μm. Each image was obtained under the same intensity settings.

visualized by incorporation of 0.5 mol% DiD, a dye that distributes preferentially into the Ld phase [36].

When R8-Alexa (1.5 μM) was incubated with the respective GUVs for 1 h, no significant accumulation of R8-Alexa was observed on the membranes of neutral GUVs composed of DOPC/SM/Chol (2:2:1) (Fig. 1A). In contrast, a marked R8-Alexa peptide signal was observed on the membranes of DOPC/DOPS/SM/Chol (1:1:2:1) GUVs containing DOPS as a negatively charged lipid (Fig. 1B). However, judging by the difference in R8-Alexa signal levels inside and outside of GUVs, the internalization of R8-Alexa was not significant, even in the case of the latter GUVs.

Heterogeneous signal distributions of DiD on both neutral and negatively charged GUV membranes were observed, and more distinct phase separation was observed for the DOPC/DOPS/SM/Chol (1:1:2:1) GUVs (Fig. 1A and B) — the phase separation of the DOPC/SM/Chol (2:2:1) GUVs was more evident when the CLSM was focused on the surface of the GUVs instead of the equatorial plane (Fig. 1A, right). The signals of R8-Alexa accumulated on DOPC/DOPS/SM/Chol (1:1:2:1) GUVs well colocalized with those of DiD, suggesting preferential localization of R8-Alexa on the Ld phase (Fig. 1B, arrows). These results are in agreement with previous findings [22] regarding the HIV-1 TAT peptide, another representative arginine-rich CPP [5,37].

Previously, we reported that modification of the N-terminus of R8 with hexanoic acid resulted in enhanced peptide interaction with plasma membranes, which promoted direct penetration of R8 through the membranes [38]. In the current study, we evaluated the modes of interaction of Alexa-labeled hexanoyl-R8 (hexanoyl-R8-Alexa) with GUVs in comparison with those of R8-Alexa (Fig. S1). Similar to R8-Alexa, hexanoyl-R8-Alexa showed preferential adsorption onto the Ld phase of negatively charged GUVs (Fig. S1A). However, R8-Alexa showed little membrane penetration through DOPC/DOPS/SM/Chol (1:1:2:1) GUV membranes 1 h after peptide administration (Fig. 1B and the lower panels in Fig. S1C), whereas time-dependent increase in internalized hexanoyl-R8-Alexa signals in GUVs was observed (Fig. S1B and C). Judged by confocal microscopic observation, hexanoyl-R8-Alexa reached the inside of more than half of GUVs with the same lipid composition in 30 min, yielding no substantive differences in signal intensities inside and outside of the membranes (upper panels in Fig. S1C). Line intensity profiles of DiD and Alexa signals confirmed this observation (right panels in Fig. S1C; note that DiD also serves as a lipid marker in this experiment). Thus, enhancement of the peptide–membrane interaction may promote membrane translocation of R8.

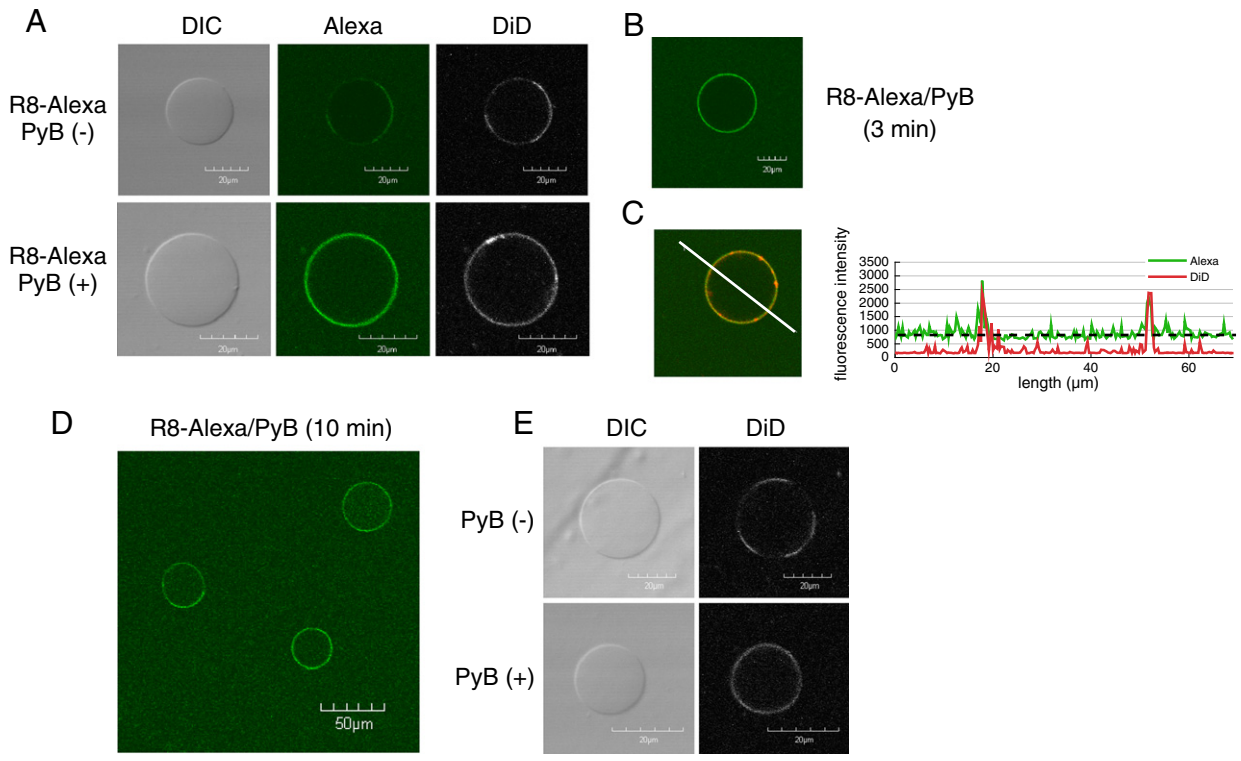

Fig. 2. (A) CLSM observation of GUVs composed of DOPC/DOPS/SM/Chol (1:1:2:1). (A) GUVs were treated with R8-Alexa (1.5 μM) in the presence and absence of PyB (15 μM) for 15 min. (B) Alexa-R8 signals were observed on GUV membranes beginning 3 min after addition of R8-Alexa (1.5 μM) and PyB (15 μM). (C) Significant internalization of R8-Alexa accompanied its surface adsorption on GUVs 5 min after addition of R8-Alexa and PyB (left). The panel on the right side represents the intensity profiles of Alexa (green) and DiD (red) signals along the lines on the confocal pictures on the left. The lack of difference in Alexa signal intensity inside and outside GUVs suggested the completion of internalization of R8-Alexa at this time point. (D) This was further confirmed by the fact that all GUVs showed internalized R8-Alexa after 10 min when cotreated with PyB. (E) Inhibition of phase separation of GUVs by addition of PyB. GUVs having Ld/Lo phase separation were treated with or without PyB (15 μM) for 15 min. All GUVs contain 0.5 mol% DiD as a Ld-phase marker, which was also regarded as a lipid marker in this experiment. Scale bars, 20 μm (A, B, and E), and 50 μm (D), respectively.

3.2. Addition of PyB leads to enhancement of peptide–membrane interactions

Next, we examined the effects of PyB on the peptide–lipid interaction. The R8-Alexa/PyB ratio was set at 1:10, considering that R8 possesses eight guanidino-functions in one molecule that potentially form pairs with PyB and mimicking the condition necessary for efficient translocation of R8-Alexa through plasma membranes into cells [10]. While DOPC/DOPS/SM/Chol (1:1:2:1) GUVs exhibited a marked accumulation of R8 on their Ld phase (Fig. 1A), the addition of PyB accelerated R8-Alexa accumulation on the membranes (Fig. 2A).[1] More than 30 min was needed to detect significant R8-Alexa signals on the membranes of DOPC/DOPS/SM/Chol (1:1:2:1) GUVs in the absence of PyB under the given conditions. In contrast, R8-Alexa signals were observed on the membrane as early as 3 min after peptide treatment of GUVs in the presence of PyB (Fig. 2B). Moreover, significant internalization of R8-Alexa accompanied its surface adsorption on DOPC/DOPS/SM/Chol (1:1:2:1) GUVs; as determined by means of line intensity profiles of Alexa signals, there were no substantive differences in Alexa signals inside and outside of GUVs after 5 min (Fig. 2C). At 10 min after peptide administration, almost all GUVs showed internalized R8-Alexa, with very little membrane perturbation (Fig. 2D). Therefore, the addition of PyB accelerates the accumulation of R8-Alexa on DOPC/DOPS/SM/Chol (1:1:2:1) GUV surfaces and its internalization into GUVs. In contrast, when neutral GUVs composed of DOPC/SM/Chol (2:2:1) were employed, neither significant accumulation of R8-Alexa on the GUV surfaces, nor internalization, occurred even in the presence of PyB 1 h after peptide addition (data not shown). These findings suggest the importance of both negatively charged lipids and PyB for efficient internalization of R8-Alexa into GUVs.

The ability of PyB to enhance peptide–membrane interaction was further evaluated by fluorescence anisotropy decay analysis of R8-BODIPY on DOPC 100% and DOPC/DOPS (3:1) LUVs (Table 1). Tight interaction between the peptide and the membrane may reduce the mobility of the fluorescent probe, which can be detected as the anisotropy decay change. To assess the effect of negative charges of membrane more directly, simpler systems without SM and Chol were employed. Initially, we employed R8-Alexa to evaluate anisotropy decay. However, the possible repulsion between the negative charge of the Alexa moiety and the negatively charged DOPS and PyB may have prevented sufficient interaction for evaluation of anisotropy of the Alexa moiety (data not shown). Therefore, we employed the neutral BODIPY moiety as the probe for this assay. In PBS(−) or in the presence of neutral DOPC LUVs, a 20–40% increase in the rotational correlation time (θ) of R8-BODIPY was found in the presence of PyB compared to its absence (Table 1). In the presence of DOPC/DOPS (4:1) LUVs, the average θ value was two to three times higher than those in PBS(−) or in the presence of DOPC 100% LUVs, even in the absence of PyB, which was doubled upon addition of PyB (Table 1). The above results support the contribution of negatively charged lipids in binding of the R8 peptide on the membrane, as well as the synergic effect of PyB.

[1] Additionally, although the addition of premixed PyB and R8-Alexa to GUVs or the addition of PyB prior to R8-Alexa also resulted in R8-Alexa adsorption onto DOPC/DOPS/SM/Chol (1:1:2:1) GUVs and their internalization, addition of R8-Alexa prior to PyB, as above, resulted in the most efficient R8-Alexa adsorption onto, and internalization into, GUVs. Membrane unbound pyrenebutyrate may compete with negatively charged GUV surfaces, inhibiting the attachment of R8-Alexa to the surface. However, the reason for the differences in the internalization efficiency of R8-Alexa resulting from the order of addition of R8-Alexa and PyB to the GUVs is currently unclear.

Table 2
Fluorescence anisotropy of DPH.

	DPH	R8 + PyB	PyB alone
DOPC/SM/Chol (2:2:1)	0.195	0.195	0.196
DOPC/DOPS/SM/Chol (1:1:2:1)	0.205	0.160	0.160
Anisotropy at 450 nm			

3.3. PyB also increases membrane fluidity

Another notable finding is distributional alteration of the Ld phase marker, DiD (Fig. 2A). In the absence of PyB, DOPC/DOPS/SM/Chol (1:1:2:1) GUVs have distinct domains comprising Ld and Lo phases; R8-Alexa accumulated preferentially on the Ld phase, exhibiting good colocalization with DiD signals (Fig. 1B and Fig. 2A, upper panels). When DOPC/DOPS/SM/Chol (1:1:2:1) GUVs were incubated with R8-Alexa in the presence of PyB, the separation of the Ld and Lo phases became ambiguous. Ubiquitous spread of DiD and R8-Alexa signals across GUV membranes was observed with notably higher levels of R8-Alexa accumulation than in the absence of PyB (Fig. 2A, lower panels). The spread of DiD signals was also induced by the addition of PyB alone (Fig. 2E). This suggests that PyB dissipates Ld/Lo phase separation or the Lo domain, thus increasing the fluidity of the GUV membrane.

We next examined the ability of PyB to modify membrane fluidity. Membrane fluidity was evaluated based on the anisotropy in LUV membranes containing 1,6-diphenyl-1,3,5-hexatriene (DPH) [39,40]; an increase in membrane fluidity should result in decreased DPH anisotropy. Because DPH fluorescence overlaps that of R8-Alexa, we used non-labeled R8 peptide (1 μM) and PyB (10 μM) in this

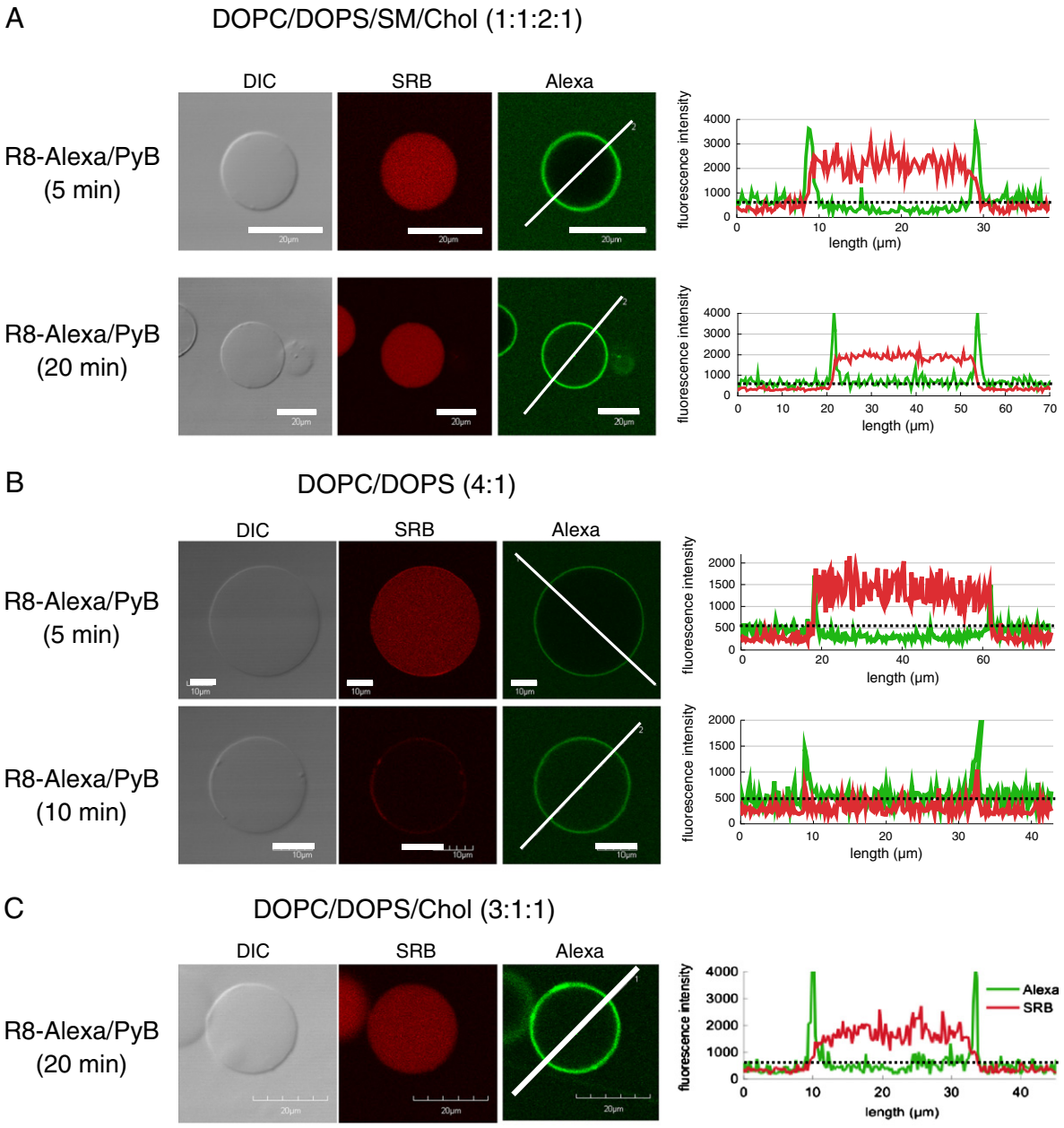

Fig. 3. No marked SRB leakage from DOPC/DOPS/SM/Chol (1:1:2:1) GUVs due to interaction with R8-Alexa (1.5 μM) in the presence of PyB (15 μM) after 20 min (A), whereas the same treatment using DOPC/DOPS (4:1) led to complete efflux of SRB in 10 min (B). However, the presence of cholesterol in the membranes prevented SRB leakage (C). Scale bars, 20 μm.

experiment (Table 2). DPH has been reported to partition equally to the Ld and Lo phases [36,41].

No anisotropy changes were observed for DOPC/SM/Chol (2:1:1) LUVs upon addition of R8 followed by PyB; however, a ~20% decrease in anisotropy occurred after identical treatment of DOPC/DOPS/SM/Chol (1:1:1:1) LUVs (Table 2, R8 + PyB). The same reduction in anisotropy was obtained using PyB alone without addition of R8 (Table 2, PyB alone). Therefore, PyB is likely the major contributor to the increased fluidity of negatively charged membranes, and is thus relevant to the disappearance of distinct Lo phases in GUV membranes of the same lipid composition. These results are also in agreement with a previous report that the TAT peptide had no significant effect on DPH anisotropy in the presence of DMPC/DMPG (3:1) LUVs [33].

3.4. Translocation of R8-Alexa through GUV membranes and membrane integrity

In the above sections, we showed the importance of the peptide–membrane interaction and membrane fluidity in promoting the adsorption and translocation of R8-Alexa, and their enhancement by PyB. R8-mediated translocation of sulforhodamine B (SRB) or membrane perturbation can be assessed by means of dye release from the vesicles [11,13,42]. We next evaluated efflux of a GUV-encapsulated fluorescent dye from the above GUVs and the effect of membrane composition on this efflux.

DOPC/DOPS/SM/Chol (1:1:2:1) GUVs containing SRB, a small, membrane-impermeable dye, were prepared and the efflux of the dye and influx of R8-Alexa was assessed by CLSM. The GUVs were treated with R8-Alexa in the presence of PyB for 20 min, leading to membrane accumulation and internalization of R8 into GUVs (Fig. 3A). While no dramatic decrease in SRB in the GUVs was observed by CLSM, detailed analysis (Fig. 3A, right) revealed a ~15% decrease in SRB signal intensity after 20 min (Fig. S2). Thus, treatment of DOPC/DOPS/SM/Chol (1:1:2:1) GUVs with R8-Alexa in the presence of PyB led to gradual SRB efflux. No decrease in SRB signals was observed for GUVs of identical composition treated with R8-Alexa or PyB alone (Fig. S2), suggesting that dye efflux was accompanied by the influx of R8-Alexa.

A more facile efflux of SRB was observed when GUVs composed of DOPC/DOPS (4:1) were employed; little SRB signal remained in the GUVs after 10 min (Fig. 3B). This may be in accordance with the recent report by Madani et al. that the addition of PyB resulted in proton efflux from a bacteriorhodopsin-incorporated POPC/POPG (4:1) LUV, used as a light-inducible endosome-mimicking system [43]. In contrast, the inclusion of cholesterol in GUV membranes prevented SRB leakage. SRB levels in DOPC/DOPS/Chol (3:1:1) GUVs were almost identical to those in DOPC/DOPS/SM/Chol (1:1:2:1) GUVs 20 min after treatment with R8-Alexa in the presence of PyB (Fig. 3C). As no significant collapse of GUVs was induced by treatment with R8-Alexa in the presence of PyB, even when this treatment was associated with marked SRB leakage, the defects in the membranes accompanied by this counteranion-mediated influx of R8-Alexa should be, if any, highly transient. Moreover, such defects likely do not comprise stable pores or extensive membrane perturbation as is often observed with basic antimicrobial peptides [44]. This is consistent with the very low cytotoxicity of intracellular delivery using R8 with the assistance of PyB. Additionally, Chol, a major component of plasma membranes, stabilizes membrane integrity during treatment with R8-Alexa in the presence of PyB, as demonstrated in this study.

3.5. Effect of PyB on membrane curvature and the implication for R8 translocation

The ability of oligoarginines, including the R8 and HIV TAT peptides, to induce membrane curvature has been hypothesized as an explanation for the translocation of these peptides [20,45–51]. Also, PyB can alter erythrocyte membrane structures [52]. If PyB can induce membrane curvature, the possible synergistic effect of R8 and PyB may be relevant to membrane translocation of R8 in the presence of PyB. GUVs composed of brain total lipid extract (BTLE) have often been employed to evaluate the effect of cytoplasmic proteins on membrane curvature formation [53]. Indeed, marked formation of inward tubular structures was observed a few minutes after addition of PyB to BTLE GUVs of this composition, and was visible after 30 min in almost all BTLE GUVs (Fig. 4A), suggesting negative curvature formation by PyB. When R8-Alexa was added to BTLE GUVs after formation of inward tubules by PyB treatment, most of the tubules disappeared after 5 min (Fig. 4B). Additionally, pretreatment of BTLE GUVs with R8-Alexa or simultaneous addition of R8-Alexa and PyB to GUVs

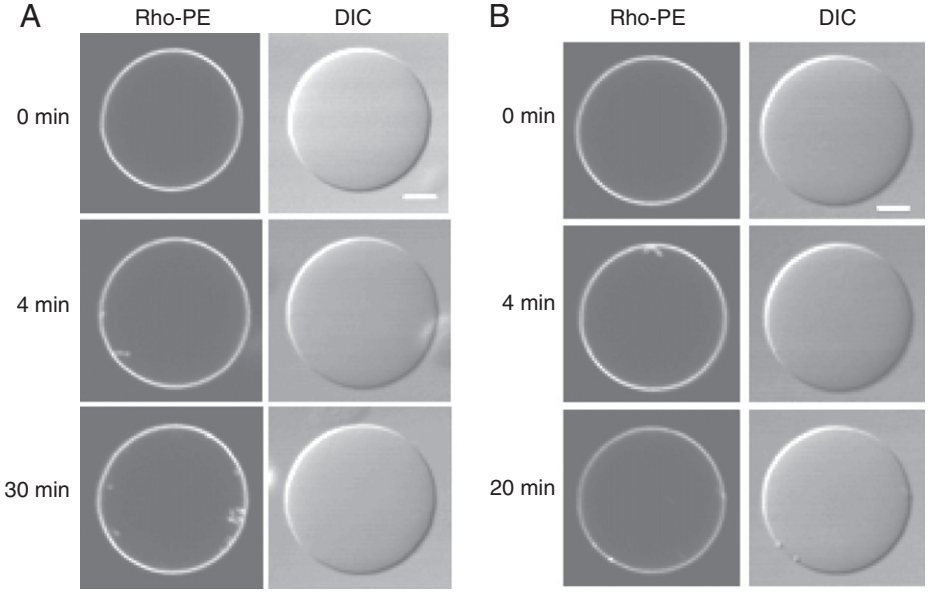

Fig. 4. CLSM observation of brain total lipid extract (BTLE) GUVs treated with PyB (15 μM) (A). In (B), R8-Alexa (1.5 μM) was added to the BTLE GUVs 5 min after the addition of PyB (15 μM). Confocal images of identical GUVs subjected to the respective conditions are shown. Time zero represents the point at which PyB was added. Rhodamine-DOPE (Rho-PE) was used as a lipid marker. Scale bars, 10 μm.

markedly suppressed the formation of the inward tubular structures (Fig. S3). Although no significant R8-Alexa influx into GUVs was observed under the conditions used, these data suggest that R8-Alexa and PyB may have reciprocal tendencies in terms of curvature formation. Simultaneous treatment with R8-Alexa and PyB may produce local and temporal deformation of the membrane, simultaneously yielding both positive and negative curvatures, which may enhance R8 translocation, as suggested by Sakamoto [45] and Wong [51] and coworkers.

4. Conclusions

In the present study, we evaluated the factors involved in PyB-mediated direct membrane translocation of R8. Confocal microscopic analyses of GUVs treated with R8-Alexa demonstrated the importance of the negatively charged lipid DOPS in R8 accumulation on the membrane; this was accelerated by PyB. Anisotropy decay measurement of R8-BODIPY also suggested the synergistic effect of anionic lipids and PyB on peptide recruitment to the membranes. Although it showed no substantive perturbation in model membranes containing SM and Chol, PyB had a marked effect on fragmentation or disappearance of the Lo phase, thus increasing membrane fluidity. The potential ability of PyB to induce negative membrane curvature was also demonstrated. Although more detailed evaluations are needed, our findings facilitate greater understanding of the unique effects of PyB in terms of promotion of R8 membrane translocation.

Acknowledgement

This work was supported in part by Grants-in-Aid for Scientific Research from the Ministry of Education, Culture, Sports, Science and Technology of Japan to I. N., Y. Y., K. M., and S. F., and S. K. is grateful for Kyoto University Education Program for Global Leaders in Advanced Engineering and Pharmaceutical Science.

Appendix A. Supplementary data

Supplementary data to this article can be found online at http://dx.doi.org/10.1016/j.bbamem.2013.05.016.

References

[1] S. Futaki, Oligoarginine vectors for intracellular delivery: design and cellular-uptake mechanisms, Biopolymers 84 (2006) 241–249.
[2] M. Mäe, U. Langel, Cell-penetrating peptides as vectors for peptide, protein and oligonucleotide delivery, Curr. Opin. Pharmacol. 6 (2006) 509–514.
[3] J.S. Wadia, S.F. Dowdy, Transmembrane delivery of protein and peptide drugs by TAT-mediated transduction in the treatment of cancer, Adv. Drug Deliv. Rev. 57 (2005) 579–596.
[4] E.A. Goun, T.H. Pillow, L.R. Jones, J.B. Rothbard, P.A. Wender, Molecular transporters: synthesis of oligoguanidinium transporters and their application to drug delivery and real-time imaging, Chem. Biochem. 7 (2006) 1497–1515.
[5] E. Vivès, P. Brodin, B. Lebleu, A truncated HIV-1 Tat protein basic domain rapidly translocates through the plasma membrane and accumulates in the cell nucleus, J. Biol. Chem. 272 (1997) 16010–16017.
[6] I.M. Kaplan, J.S. Wadia, S.F. Dowdy, Cationic TAT peptide transduction domain enters cells by macropinocytosis, J. Control. Release 102 (2005) 247–253.
[7] S. Futaki, H. Hirose, I. Nakase, Arginine-rich peptides: methods of translocation through biological membranes, Curr. Pharm. Des. 19 (2013) 2863–2868.
[8] A.T. Jones, E.J. Sayers, Cell entry of cell penetrating peptides: tales of tails wagging dogs, J. Control. Release 161 (2012) 582–591.
[9] F. Duchardt, M. Fotin-Mleczek, H. Schwarz, R. Fischer, R. Brock, A comprehensive model for the cellular uptake of cationic cell-penetrating peptides, Traffic 8 (2007) 848–866.
[10] T. Takeuchi, M. Kosuge, A. Tadokoro, Y. Sugiura, M. Nishi, M. Kawata, N. Sakai, S. Matile, S. Futaki, Direct and rapid cytosolic delivery using cell-penetrating peptides mediated by pyrenebutyrate, ACS Chem. Biol. 1 (2006) 299–303.
[11] F. Perret, M. Nishihara, T. Takeuchi, S. Futaki, A.N. Lazar, A.W. Coleman, N. Sakai, S. Matile, Anionic fullerenes, calixarenes, coronenes, and pyrenes as activators of oligo/polyarginines in model membranes and live cells, J. Am. Chem. Soc. 127 (2005) 1114–1115.
[12] K. Inomata, A. Ohno, H. Tochio, S. Isogai, T. Tenno, I. Nakase, T. Takeuchi, S. Futaki, Y. Ito, H. Hiroaki, M. Shirakawa, High-resolution multi-dimensional NMR spectroscopy of proteins in human cells, Nature 458 (2009) 106–109.
[13] N. Sakai, S. Matile, Anion-mediated transfer of polyarginine across liquid and bilayer membranes, J. Am. Chem. Soc. 125 (2003) 14348–14356.
[14] S. Futaki, Membrane-permeable arginine-rich peptides and the translocation mechanisms, Adv. Drug Deliv. Rev. 57 (2005) 547–558.
[15] I. Nakase, T. Takeuchi, G. Tanaka, S. Futaki, Methodological and cellular aspects that govern the internalization mechanisms of arginine-rich cell-penetrating peptides, Adv. Drug Deliv. Rev. 60 (2008) 598–607.
[16] C. Ciobanasu, E. Harms, G. Tünnemann, M.C. Cardoso, U. Kubitscheck, Cell-penetrating HIV1 TAT peptides float on model lipid bilayers, Biochemistry 48 (2009) 4728–4737.
[17] E. Gonçalves, E. Kitas, J. Seelig, Binding of oligoarginine to membrane lipids and heparan sulfate: structural and thermodynamic characterization of a cell-penetrating peptide, Biochemistry 44 (2005) 2692–2702.
[18] A. Ziegler, J. Seelig, Binding and clustering of glycosaminoglycans: a common property of mono- and multivalent cell-penetrating compounds, Biophys. J. 94 (2008) 2142–2149.
[19] M. Kosuge, T. Takeuchi, I. Nakase, A.T. Jones, S. Futaki, Cellular internalization and distribution of arginine-rich peptides as a function of extracellular peptide concentration, serum, and plasma membrane associated proteoglycans, Bioconjug. Chem. 19 (2008) 656–664.
[20] H. Hirose, T. Takeuchi, H. Osakada, S. Pujals, S. Katayama, I. Nakase, S. Kobayashi, T. Haraguchi, S. Futaki, Transient focal membrane deformation induced by arginine-rich peptides leads to their direct penetration into cells, Mol. Ther. 20 (2012) 984–993.
[21] A. Lamazière, O. Maniti, C. Wolf, O. Lambert, G. Chassaing, G. Trugnan, J. Ayala-Sanmartin, Lipid domain separation, bilayer thickening and pearling induced by the cell penetrating peptide penetratin, Biochim. Biophys. Acta 1798 (2010) 2223–2230.
[22] P. Säälik, A. Niinep, J. Pae, M. Hansen, D. Lubenets, Ü. Langel, M. Pooga, Penetration without cells: membrane translocation of cell-penetrating peptides in the model giant plasma membrane vesicles, J. Control. Release 153 (2011) 117–125.
[23] I. Nakase, A. Tadokoro, N. Kawabata, T. Takeuchi, H. Katoh, K. Hiramoto, M. Negishi, M. Nomizu, Y. Sugiura, S. Futaki, Interaction of arginine-rich peptides with membrane-associated proteoglycans is crucial for induction of actin organization and macropinocytosis, Biochemistry 46 (2007) 492–501.
[24] M. Magzoub, A. Pramanik, A. Gräslund, Modeling the endosomal escape of cell-penetrating peptides: transmembrane pH gradient driven translocation across phospholipid bilayers, Biochemistry 44 (2005) 14890–14897.
[25] B. Albarran, R. To, P.S. Stayton, A TAT–streptavidin fusion protein directs uptake of biotinylated cargo into mammalian cells, Protein Eng. Des. Sel. 18 (2005) 147–152.
[26] R. Pantoja, E.A. Rodriguez, M.I. Dibas, D.A. Dougherty, H.A. Lester, Single-molecule imaging of a fluorescent unnatural amino acid incorporated into nicotinic receptors, Biophys. J. 96 (2009) 226–237.
[27] K.S. Horger, D.J. Estes, R. Capone, M. Mayer, Films of agarose enable rapid formation of giant liposomes in solutions of physiologic ionic strength, J. Am. Chem. Soc. 131 (2009) 1810–1819.
[28] Y. Yano, K. Matsuzaki, Membrane insertion and dissociation processes of a model transmembrane helix, Biochemistry 41 (2002) 12407–12413.
[29] J.R. Lakowicz, Principles of Fluorescence Spectroscopy, Third ed. Springer, New York, 1999. 383–412.
[30] C. Ciobanasu, J.P. Siebrasse, U. Kubitscheck, Cell-penetrating HIV1 TAT peptides can generate pores in model membranes, Biophys. J. 99 (2010) 153–162.
[31] P.W. Thorén, D. Persson, E.K. Esbjörner, M. Goksör, P. Lincoln, B. Nordén, Membrane binding and translocation of cell-penetrating peptides, Biochemistry 43 (2004) 3471–3489.
[32] A. Ziegler, X.L. Blatter, A. Seelig, J. Seelig, Protein transduction domains of HIV-1 and SIV TAT interact with charged lipid vesicles. Binding mechanism and thermodynamic analysis, Biochemistry 42 (2003) 9185–9194.
[33] V. Tiriveedhi, P. Butko, A fluorescence spectroscopy study on the interactions of the TAT-PTD peptide with model lipid membranes, Biochemistry 46 (2007) 3888–3895.
[34] E. Sezgin, I. Levental, M. Grzybek, G. Schwarzmann, V. Mueller, A. Honigmann, V.N. Belov, C. Eggeling, U. Coskun, K. Simons, P. Schwille, Partitioning, diffusion, and ligand binding of raft lipid analogs in model and cellular plasma membranes, Biochim. Biophys. Acta 1818 (2012) 1777–1784.
[35] M. Stöckl, P. Fischer, E. Wanker, A. Herrmann, Alpha-synuclein selectively binds to anionic phospholipids embedded in liquid-disordered domains, J. Mol. Biol. 375 (2008) 1394–1404.
[36] T. Baumgart, G. Hunt, E.R. Farkas, W.W. Webb, G.W. Feigenson, Fluorescence probe partitioning between Lo/Ld phases in lipid membranes, Biochim. Biophys. Acta 1768 (2007) 2182–2194.
[37] A.D. Frankel, C.O. Pabo, Cellular uptake of the tat protein from human immunodeficiency virus, Cell 55 (1988) 1189–1193.
[38] S. Katayama, H. Hirose, K. Takayama, I. Nakase, S. Futaki, Acylation of octaarginine: Implication to the use of intracellular delivery vectors, J. Control. Release 149 (2011) 29–35.
[39] A.G. Macdonald, K.W. Wahle, A.R. Cossins, M.K. Behan, Temperature, pressure and cholesterol effects on bilayer fluidity; a comparison of pyrene excimer/monomer ratios with the steady-state fluorescence polarization of diphenylhexatriene in liposomes and microsomes, Biochim. Biophys. Acta 938 (1988) 231–242.
[40] J.R. Lakowicz, Principles of Fluorescence Spectroscopy, Third ed. Springer, New York, 1999. 353–382.
[41] M. Omar Bakht, E. London, Cholesterol precursors stabilize ordinary and ceramide-rich ordered lipid domains (lipid rafts) to different degrees. Implications for the Bloch hypothesis and sterol biosynthesis disorders, J. Biol. Chem. 281 (2006) 21903–21913.

[42] P. Guterstam, F. Madani, H. Hirose, T. Takeuchi, S. Futaki, S. El Andaloussi, A. Gräslund, Ü. Langel, Elucidating cell-penetrating peptide mechanisms of action for membrane interaction, cellular uptake, and translocation utilizing the hydrophobic counter-anion pyrenebutyrate, Biochim. Biophys. Acta 1788 (2009) 2509–2517.
[43] F. Madani, R. Abdo, S. Lindberg, H. Hirose, S. Futaki, Ü. Langel, A. Gräslund, Modeling the endosomal escape of cell-penetrating peptides using a transmembrane pH gradient, Biochim. Biophys. Acta 1828 (2013) 1198–1204.
[44] K. Matsuzaki, O. Murase, N. Fujii, K. Miyajima, An antimicrobial peptide, magainin 2, induced rapid flip-flop of phospholipids coupled with pore formation and peptide translocation, Biochemistry 35 (1996) 11361–11368.
[45] K. Sakamoto, K. Aburai, T. Morishita, K. Sakai, H. Sakai, M. Abe, I. Nakase, S. Futaki, Bioinspired mechanism for the translocation of peptide through the cell membrane, Chem. Lett. 41 (2012) 1078–1080.
[46] S. Yesylevskyy, S.J. Marrink, A.E. Mark, Alternative mechanisms for the interaction of the cell-penetrating peptides penetratin and the TAT peptide with lipid bilayers, Biophys. J. 97 (2009) 40–49.
[47] A. Mishra, V.D. Gordon, L. Yang, R. Coridan, G.C. Wong, HIV TAT forms pores in membranes by inducing saddle-splay curvature: potential role of bidentate hydrogen bonding, Angew. Chem. Int. Ed. Engl. 47 (2008) 2986–2989.
[48] A. Lamazière, C. Wolf, O. Lambert, G. Chassaing, G. Trugnan, J. Ayala-Sanmartin, The homeodomain derived peptide penetratin induces curvature of fluid membrane domains, PLoS One 3 (2008) e1938.
[49] S. Afonin, A. Frey, S. Bayerl, D. Fischer, P. Wadhwani, S. Weinkauf, A.S. Ulrich, The cell-penetrating peptide TAT (48–60) induces a non-lamellar phase in DMPC membranes, ChemPhysChem 7 (2006) 2134–2142.
[50] I.D. Alves, N. Goasdoué, I. Correia, S. Aubry, C. Galanth, S. Sagan, S. Lavielle, G. Chassaing, Membrane interaction and perturbation mechanisms induced by two cationic cell penetrating peptides with distinct charge distribution, Biochim. Biophys. Acta 1780 (2008) 948–959.
[51] N.W. Schmidt, M. Lis, K. Zhao, G.H. Lai, A.N. Alexandrova, G.N. Tew, G.C. Wong, Molecular basis for nanoscopic membrane curvature generation from quantum mechanical models and synthetic transporter sequences, J. Am. Chem. Soc. 134 (2012) 19207–19216.
[52] E. Alhanaty, M.P. Sheetz, Control of the erythrocyte membrane shape: recovery from the effect of crenating agents, J. Cell Biol. 91 (1981) 884–888.
[53] H. Chen, S. Fre, V.I. Slepnev, M.R. Capua, K. Takei, M.H. Butler, P.P. Di Fiore, P. De Camilli, Epsin is an EH-domain-binding protein implicated in clathrin-mediated endocytosis, Nature 394 (1998) 793–797.